ISSN 0015-4628, Fluid Dynamics, 2019, Vol. 54, no. 6, pp. 821–834. © Pleiades Publishing, Ltd., 2019.
Russian Text © The Author(s), 2019, published in Izvestiya RAN. Mekhanika Zhidkosti i Gaza, 2019, No. 6, pp. 84–97.

Global Stability Analysis of Spatially Developing Boundary Layer: Effect of Streamwise Pressure Gradients

Ramesh Bhoraniya[a],* and Vinod Narayanan[b]

[a] *Department of Mechanical Engineering, Marwadi Education Foundation Group of Institutions, Rajkot, India*

[b] *Department of Mechanical Engineering, Indian Institute of Technology Palaj, Gandhinagar, India*

** e-mail: rameshbhoraniya@gmail.com*

Received January 15, 2019; revised February 15, 2019; accepted March 20, 2019

Abstract—The paper presents a global stability analysis of the two-dimensional incompressible boundary layer with the effect of streamwise pressure gradient. A symmetric wedge flow is considered at different values of the dimensionless pressure gradient parameter β_H. The pressure gradient dp/dx in the flow direction is zero, when $\beta_H = 0$, favorable (negative) for $\beta_H > 0$, and adverse (positive) for $\beta_H < 0$. The base flow is computed by numerical solution of Falkner—Skan equation. The Reynolds number is based on the displacement thickness δ^* at the inflow boundary. The stability equations governing the flow are derived in body-fitted coordinates. The stability equations are discretized using the Chebyshev spectral collocation method. The discretized equations, together with boundary conditions, form a general eigenvalue problem and are solved using Arnoldi's algorithm. The temporal global modes are computed for $\beta_H = 0.022$, 0.044, and 0.066, for favorable and adverse pressure gradients. The temporal growth rate ω_i is found to be negative for all the global modes. The ω_i value is smaller for the favorable pressure gradient (FPG) than for the adverse pressure gradient (APG) at the same Reynolds number (Re = 340). Thus, the FPG has a stabilizing effect on the boundary layer. The comparison of the spatial eigenmodes and spatial amplification rates for FPG and APG show that FPG has a stabilizing effect, whereas APG has a destabilizing effect on the disturbances.

Keywords: boundary layer, incompressible fluid, streamwise pressure gradient, global stability, numerical solutions

DOI: 10.1134/S0015462819060028

The boundary layers developing on solid surfaces are generally laminar near the leading edges. As the distance from the leading edge increases, the Reynolds number also increases. The Reynolds number, at which transition to turbulence occurs, is known as the critical Reynolds number. The region, over which the flow transition takes place, is known as the transition zone or transition length. At very low free-stream turbulence levels the transition is characterized by the Tollmien—Schlichting (TS) wave mechanism. The process of transition initiates with the random amplification of small disturbances. The standard procedure to predict the transition onset is to compute the growth of the small disturbances within the laminar region. The instability/growth of the small disturbances is the very first step of the transition process. Many factors are known to affect the transition process, e.g., free-stream turbulence, streamwise pressure gradient (PG), streamwise curvatures, surface roughness, etc. Knowledge of the transition process is beneficial, where the turbulence is necessary to be avoided, but also where the turbulence might be desirable to promote, for instance, better fluid mixing to manage turbulence efficiently. There is a strong relation between transition and flow separation, which is a non-desirable phenomenon in most of engineering applications. Therefore, understanding the transition can lead to a better control of flow separation. The study of the PG effect on the flow instability is of specific interest because it is one of the passive flow control devices. The previous studies of the effect of PG showed that FPG increases the critical Reynolds number of incompressible boundary layers, whereas APG has an opposite effect. Flows through turbomachinery and airplane wings are the engineering applications, where the streamwise PG exists. The linear stability analysis of parallel flows shows that disturbances amplify more rapidly in the case of boundary layers with adverse pressure gradients (APG). Sometimes, transition can happen within the zone of a favorable pressure gradient (FPG), for example, in flows past low-pressure turbine and compressor blades at high free-stream turbulence level.

Obremski et al. showed that a FPG stabilizes an incompressible boundary layer, whereas the APG effect is opposite [1]. The flight test data reported by Driest [2] indicate that an increase in FPG increases the transition Reynolds number. The flow with very strong APG is known to have an inflection point and is inviscidly unstable. In inviscid flows, velocity profile with inflection point can always be shown to be unstable with respect to the Rayleigh criterion. The streamwise PG crucially affects the growth of small disturbances. A FPG leads to a fuller velocity profile with a relatively lower shape factor and thus has a stabilizing impact, whereas an APG results in more significant amplification rate of disturbance waves. Saxena and Bose [3] investigated that the FPG stabilizes the flow and APG destabilizes the flow.

A strong APG promotes boundary layer separation and speeds up the process of transition to turbulence. Such boundary layers are much more unstable than the flat-plate boundary layers. Corke and Gruber [4] experimentally studied the resonant growth of a triad of instability waves consisting of a plane TS mode and a pair of oblique modes with the same and opposite wave angles, which are undergoing subharmonic transition in Falkner—Skan boundary layers with the APG parameter in the range $0 \geqslant \beta_H \geq -0.09$. Although large instabilities did not occur in their experiments, the transition process was observed to differ considerably from the Blasius case in many aspects. For example, the streamwise extent of the amplitude saturation was extremely short compared to the Blasius layer and the maximum amplitudes reached by the sub-harmonic modes in their cases were twice as large as those in the Blasius layer with comparable initial conditions. The simulations of Liu and Maslowe [5] revealed that the sub-harmonic three-dimensional waves are most dangerous in the APG. Here also, amplification rates are found to be much greater than in the Blasius flow. Consequently, transition sets in at a considerably lower Reynolds number in the decelerating boundary layers. The transition zone is much shorter and transition onset is upstream in the APG boundary layers. Abu-Ghannam and Gostelow et al. [6, 7] found experimentally higher spot inception and spreading rates in the decelerated flows. Vinod and Govindarajan [8, 9] showed that there exists a direct connection between the pattern of breakdown of turbulent spots and the laminar instability characteristics in the strong APG boundary layers. Narasimha and Seifert and Hodson [10, 11] experimentally found that the growth of the turbulent spots in the downstream direction is self-similar irrespective of the type of PG. It maintains an arrowhead shape in the top view and follows self-similar growth of the spot size. Maslowe and Spiteri [12] reported the behavior of the eigen-solutions of a continuous spectrum for a boundary layer subjected to a PG in the flow direction. They found larger disturbance amplitudes compared to the Blasius flow in an APG boundary layer. The possibilities of the secondary instabilities are higher close to the edge of boundary layer because of massive shear rate. The spatial amplification rate α_i is also smaller than that of the Blasius flow. The magnitude of eigenfunctions could be larger than in the Blasius flow even when the PG is favorable. However, the transition Reynolds number is higher and thus α_i is also large. Zurigat et al. [13] in their investigation of compressible boundary layers found that FPG has a stabilizing and APG has a destabilizing effect on the 2D second waves. The effectiveness of the FPG reduces at hypersonic Mach numbers. It is clear that FPG pressure gradients are stabilizing, whereas APG are destabilizing in boundary layers. Thus, boundary layers subjected to FPG and APG are stable and unstable, respectively. The band of frequencies widens to amplify the disturbances with APG for incompressible boundary layers. Franko and Lele [14] found completely different transition eventualities with APG for high-speed boundary layers. They applied APG through free-stream condition and found that APG fails to essentially modify the transition pattern. However, it quickens transition and ends up in the upper rate for first and second mode instabilities. The transition was analogous to ZPG for the soft APG boundary layers. Zhang et al. [15] performed a global stability computation for 2D flow past an inclined triangular cylinder. They found that the spatial structure of the disturbances is nearly similar for $\alpha \leq 30^\circ$ and the temporal growth rate is sensitive to near wake flow, whereas for $\alpha \leq 40^\circ$ there are exceptional transverse growth and streamwise elongation of the disturbances and the growth rate is sensitive to far-wake flow.

Kimmel [16] experimentally found that the transition zone length was 1.7 to 2.0 times shorter for FPG compared to ZPG in hypersonic boundary layers. The APG promoted earlier transition and the Reynolds number at the end of the transition zone was higher than in the ZPG case. The transition zone length trends are opposite to subsonic trends. Itoh [17] investigated the PG effect in two directions and the effect of the sweep angle of a wing on the stability of three-dimensional boundary layers. It was found that in the region of streamwise FPG an appropriate choice of the PG can restrain the cross-flow on a very weak level, thus stabilizing the boundary layer by a higher critical Reynolds number. Johnson and Pinarbasi [18] numerically studied the effect of ZPG, FPG, and APG on the receptivity of the 3D boundary layers. It was found that the boundary layer is receptive only in a narrow band of spanwise wavelengths ranging from one to four times the local boundary layer thickness. The receptivity of APG is twice as large as that of FPG. The significant TS wave activity was found for APG only. However, it was also detected for ZPG.

Masad and Zurigat [19] investigated the effect PG on the first mode instability of the subsonic and supersonic compressible boundary layers at Mach numbers from 0 to 7. Variations of maximum growth rate for different levels of FPG and APG with different edge Mach numbers have been computed. The FPG has a stabilizing effect on the first mode. However, at high edge Mach numbers the FPG effect is less stabilizing. The frequency and spanwise and streamwise wave numbers corresponding to the maximum growth rate decrease with increase in the FPG. Tumin and Ashpis [20] found that FPG reduces the non-modal growth, while APG leads to an increase in the amplification. Gostelow and Blunden [21] developed an intermittancy meter that permits the online monitoring for about 100 s. The results of four different turbulence levels for ZPG were well confirmed by the previous results. The transition region length was found to be long without any PG while for APG strong reduction in transition length was found. The turbulent spot formation rate increased. Igarashi et al. [22] experimentally investigated that for half included angle of 3.6° the transition process was different from the case of ZPG. The amplification rate for $\theta = 3.6°$ was found almost one order higher than that for $\theta = 0$. This suggests that transition of boundary layer to turbulent state is a consequence of the instability of the laminar boundary layer. It was observed that the frequency spectrum at transition was white for $\theta = 0$ and nonwhite for large APG. Govndarajan and Narasimha [23] presented a new formulation for the boundary layer stability with the existence of PG. They assumed that the disturbance wavelength and eigenfunction vary no more rapidly than the boundary layer thickness. A strong APG has a significant destabilizing effect on the boundary layer. The effect of nonparallelism on the high frequencies can be significant at low Reynolds number. Walker and Gostelow [24] reviewed all existing transition models and deficiencies in the prediction of the transition length under APG. They proposed a new model for transition which included the effect of both Reynolds number and APG with the experimental validation. They found that, as the APG increases from zero to separation values, TS waves evolve from random to periodic behavior and the transition length progressively reduces. Chonghui [25] performed direct numerical simulation (DNS) of spatial instabilities with the normal mode for the Falkner—Skan velocity profiles (APG). He found the maximum streamwise disturbance velocity amplitudes are 10–20% higher towards the downstream end of the domain than that in the experimental measurement of Corke et al. [4]. For small APG, $\beta_H = -0.06$, the disturbances were not shown to exhibit explosive instability. However, for $\beta_H = -0.15$, the disturbances were shown to amplify dramatically. The reason was that the critical layer is farther away from the wall with larger APG. Corbett and Bottaro [26] studied the algebraic growth mechanism in the Falkner—Skan boundary layer using the direct-adjoint technique. The APG was found to increase the resulting growth of the disturbances and reverse for FPG. It was found that disturbances producing maximum amplification over a shorter period are generally oblique and can experience significant transient growth. The main aim of this paper is to study the impact of the streamwise PG on the global instability of boundary layers. The PG impact on the boundary layers was studied in the past using the local stability approach in which the streamwise variation of the base flow is neglected and disturbance amplitudes are functions of wall normal direction only. The global modes were computed for ZPG boundary layers in the past by some investigators [27—29]. Bhoraniya and Vinod [30—32] in their study on axisymmetric boundary layers found that the transverse curvature and FPG have a stabilizing effect. Thus, this was the first attempt to compute the global modes of the two-dimensional boundary layers subjected to streamwise PG.

1. FORMULATION OF THE PROBLEM

We will consider an incompressible flow over a symmetric wedge with different values of β_H for FPG and APG. Thus, the incoming flow has some incident angle with the symmetry line of the wedge. The base flow is two-dimensional and non-parallel. The standard procedure is adopted to derive Navier—Stokes equations for disturbances. The governing stability equations are normalized using U_∞ and δ^*. The Reynolds number is based on the δ^* value at the entry of the domain x_{in}, as shown in Fig. 1. The two-dimensional eigenvalue problem is solved for an instability analysis of the 2D boundary layer. In the present analysis, two-dimensional disturbances considered.

The Reynolds number

$$\text{Re} = \frac{U_\infty \delta^*}{\nu}. \tag{1.1}$$

The flow quantities are split into the base flow and perturbations as follows:

$$\bar{U} = U_b + u_p, \quad \bar{V} = V_b + v_p, \quad \bar{P} = P_b + p_p, \tag{1.2}$$

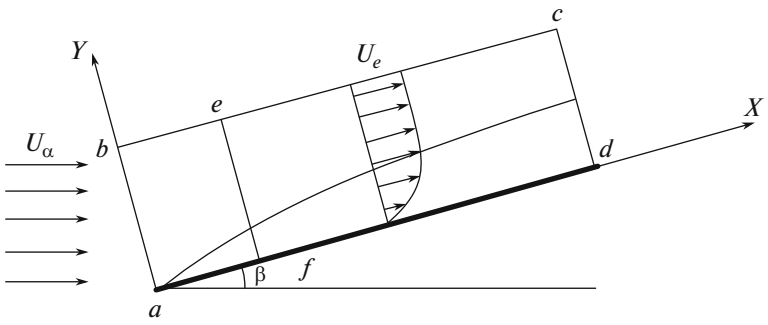

Fig. 1. Spatially developing incompressible boundary layer on an inclined flat plate. The incident angle β_H develops PG in the streamwise direction. A positive value of β_H measured in the counterclockwise direction gives FPG, while its negative value results in APG.

where $\bar{U}$, $\bar{V}$, and $\bar{P}$ are the instantaneous values of the parameters, U_b, V_b, and P_b are the baseline flow parameters, and u_p, v_p, and p_p are disturbances.

We assume normal mode form of the disturbances with the amplitudes varying in the wall normal y and streamwise x directions

$$u_p(x,y,t) = \hat{u}_p(x,y)e^{-i\omega t}, \quad v_p(x,y,t) = \hat{v}_p(x,y)e^{-i\omega t}, \quad p_p(x,y,t) = \hat{p}_p(x,y)e^{-i\omega t}. \tag{1.3}$$

The linearized Navier—Stokes equations for an instability analysis are as follows:

$$\frac{\partial u_p}{\partial t} + U_b\frac{\partial u_p}{\partial x} + u_p\frac{\partial U_b}{\partial x} + V_b\frac{\partial u_p}{\partial y} + v_p\frac{\partial U_b}{\partial y} + \frac{\partial p_p}{\partial x} - \frac{1}{\mathrm{Re}}[\nabla^2 u_p] = 0, \tag{1.4}$$

$$\frac{\partial v_p}{\partial t} + U_b\frac{\partial v_p}{\partial x} + u_p\frac{\partial V_b}{\partial x} + V_b\frac{\partial v_p}{\partial y} + v_p\frac{\partial V_b}{\partial y} + \frac{\partial p_p}{\partial y} - \frac{1}{\mathrm{Re}}[\nabla^2 v_p] = 0, \tag{1.5}$$

$$\frac{\partial u_p}{\partial x} + \frac{\partial v_p}{\partial y} = 0, \tag{1.6}$$

where

$$\nabla^2 = \frac{\partial^2}{\partial x^2} + \frac{\partial^2}{\partial y^2}. \tag{1.7}$$

1.1. Boundary Conditions

The u_p and v_p disturbances have zero magnitudes (no slip and no penetration) on the solid surface because of the viscous effect

$$u_p(x,0) = 0, \quad v_p(x,0) = 0. \tag{1.8}$$

The disturbance amplitudes decay exponentially and vanish in the far field, away from the wall. Thus, all disturbance velocity components and pressure are taken to be zero in the far field.

$$u_p(x,\infty) = 0, \quad v_p(x,\infty) = 0, \quad p_p(x,\infty) = 0. \tag{1.9}$$

We will study the growth or decay of the small disturbances within the considered flow domain under the effect of PG. Thus, all disturbance velocity components have zero magnitudes at the inflow boundary of the domain. This is consistent with the Theofilis suggestion [33]

$$u_p(x_{\mathrm{in}},y) = 0, \quad v_p(x_{\mathrm{in}},y) = 0. \tag{1.10}$$

At the exit boundary we may apply the boundary conditions based on the wave information [34]. These conditions are more restrictive in nature because they impose the wave-like behavior of the disturbances. Physically it is not a good condition for the instability analysis. The streamwise wave-number α is not known initially for the global stability analysis. An alternative way is to impose numerical boundary conditions which extrapolate the information from the interior of the computational domain. Linear extrap-

olated conditions are considered by several investigators at the outflow boundary. A review of the literature on global stability analysis suggests that linearly extrapolated boundary conditions are the most suitable boundary conditions [27, 33, 35]. Thus, we will consider the linear extrapolated conditions at the outflow boundary

$$u_{p_{n-2}}[x_n - x_{n-1}] - u_{p_{n-1}}[x_n - x_{n-2}] + u_{p_n}[x_{n-1} - x_{n-2}] = 0, \tag{1.11}$$

where x_n, x_{n-1}, and x_{n-2} are the most exterior grid points at the outlet of domain and u_p is the streamwise disturbance velocity component. Similarly, one can write extrapolated boundary conditions for the wall-normal disturbance components v_p. The compatibility conditions applied for the pressure at the solid wall derived are from the stability equations themselves [33]

$$\frac{\partial p_p}{\partial x} = \frac{1}{\mathrm{Re}}\frac{\partial^2 u_p}{\partial y^2}, \tag{1.12}$$

$$\frac{\partial p_p}{\partial y} = \frac{1}{\mathrm{Re}}\frac{\partial^2 v_p}{\partial y^2}. \tag{1.13}$$

The primitive variable approach was applied in the derivation of the stability equations. The advantage of the primitive variable formulation over the high-order numerical approach is that only the first derivatives of the base flow and the second derivatives of the disturbance flow quantities appear. The lower-order derivatives give smaller discretization errors at the modest resolution. The governing equations (1.4) and (1.5) are discretized using the Chebyshev polynomials in both spatial directions. The Chebyshev polynomials generate non-uniform grid points with a greater of collocation points towards both ends.

$$x_{\mathrm{cheb}} = \cos\left(\frac{\pi i}{n}\right) \quad \text{for} \quad i = 0,1,2,3\ldots.n. \tag{1.14}$$

$$y_{\mathrm{cheb}} = \cos\left(\frac{\pi j}{m}\right) \quad \text{for} \quad j = 0,1,2,3\ldots.m. \tag{1.15}$$

The gradients of the disturbance amplitude functions are very large in the wall region within the thin boundary layer, which requires a large number of grid points to increase the spatial resolution. Grid stretching is applied via the following algebraic equation [36]

$$y_{\mathrm{real}} = \frac{y_i L_y(1 - y_{\mathrm{cheb}})}{L_y + y_{\mathrm{cheb}}(L_y - 2y_i)}. \tag{1.16}$$

In the above grid stretching method, half number of the collocation points are concentrated within the y_i distance from the lower boundary. The nonuniform nature of the collocation point distribution in the streamwise direction is undesirable. The maximum and minimum distances between the grid points are at the center and at the end, respectively. Thus, it makes a poor resolution at the center of the domain and a very small distance between the grids at the end gives rise to the Gibbs phenomenon. To improve the resolution and to minimize the Gibbs oscillations in the solution, the grid mapping is implemented in streamwise direction using the following algebraic equation [37]

$$x_{\mathrm{map}} = \frac{\arcsin(\alpha_m x_{\mathrm{cheb}})}{\arcsin(\alpha_m)}. \tag{1.17}$$

The value of α_m is selected carefully to improve the spatial resolution in the streamwise direction. A very small value of α_m keeps the grid distribution similar with the Chebyshev distribution, while a near-unity value provides an almost uniform grid. For the detail description of the grid mapping, readers are suggested to refer [37]. To incorporate the effect of physical dimensions of the domain [L_x, L_y] along with grid stretching and mapping it is required to multiply the Chebyshev differentiation matrices by the proper Jacobean matrix. The linear operator of the discretized LNS system forms the matrices K and M. These matrices are square, real and sparse in nature and formulate general eigenvalue problem

$$\begin{bmatrix} K_{11} & K_{12} & K_{13} \\ K_{21} & K_{22} & K_{23} \\ K_{31} & K_{32} & K_{33} \end{bmatrix} \begin{bmatrix} u_p \\ v_p \\ p_p \end{bmatrix} = i\omega \begin{bmatrix} M_{11} & M_{12} & M_{13} \\ M_{21} & M_{22} & M_{23} \\ M_{31} & M_{32} & M_{33} \end{bmatrix} \begin{bmatrix} u_p \\ v_p \\ p_p \end{bmatrix}, \tag{1.18}$$

$$[K][\psi] = i\omega[M][\psi],$$

where K and M are the square matrices of size $3\,\mathrm{nm} \times 3\,\mathrm{nm}$, $i\omega$ is an eigenvalue, and ψ is the vector of unknown amplitudes of the disturbance flow quantities u_p, v_p, and p_p. The above-mentioned boundary conditions are properly incorporated in the matrices K and M. The numerical solution of Eq. (1.18) is performed using Arnoldi's iterative algorithm. Readers are suggested to refer [31, 32] for detailed description of the eigenvalue problem solution.

2. BASE FLOW SOLUTION

The Falkner—Skan velocity profile is used as the base velocity profile. The value of β_H decides whether the flow is accelerating ($\beta_H > 0$) or decelerating ($\beta_H < 0$).

$$f''' + ff'' + \beta_H(1 - f'^2) = 0. \tag{2.1}$$

The base velocity is computed by solving Eq. (2.1), together with the boundary conditions

$$\eta = 0: \quad f = f' = 0; \quad \eta \to \infty: \quad f' = 1. \tag{2.2}$$

The streamwise and normal velocity components are computed as follows:

$$U_b = U_\infty f'; \quad V_b = \frac{-1}{2}\sqrt{\frac{\nu U_\infty}{x}}[\eta f'(\eta) - f(\eta)]. \tag{2.3}$$

The numerical solution of the Eq. (2.1) is obtained using the fourth-order Runge—Kutta method.

Here, the incident angle $\beta_H = 0$ resembles the flat-plate boundary layer with ZPG; $\beta_H > 0$ develops FPG and $\beta_H < 0$ develops APG in the streamwise direction. Figures 2a, 2b, and 2c present the comparison of U_b, dU_b/dy, and d^2U_b/dy^2 for FPG, ZPG, and APG at the same streamwise location $x = 0.5$ m. The magnitude of the first derivative (dU_b/dy) is higher in the case of FPG that accelerates the flow. The magnitude of the second derivative (d^2U_b/dy^2) is found to be negative for FPG and positive for the APG. The negative value of d^2U_b/dy^2 with the FPG, whereas the positive value of d^2U_b/dy^2 increases with the APG. We note that the negative d^2U_b/dy^2 have stabilizing and positive d^2U_b/dy^2 have a destabilizing effect.

3. RESULTS AND DISCUSSION

In the present stability analysis the flat-plate boundary layer with the existence of streamwise PG is considered. The semi-wedge angles β_H equal to 0.022, 0.0444, and 0.0667 are considered, which in turn develop PG in the direction of flow. We consider both positive (FPG) and negative (APG) values of angle β_H. Three values of Reynolds number, 340, 416, and 480, are considered based on the δ^* at the inflow boundary. The linear dimensions in both directions are normalized by the δ^*. The domain height in the wall-normal direction is taken as $20\delta^*$, that is, twenty times the δ^* at the inflow boundary. It is sufficiently large value and has no influence on the results [27]. The number of collocation points considered in the direction of flow and the normal direction are 251 and 61, respectively. The temporal and spatial characteristics of the least stable eigenmodes are studied. The convergence of the solution was additionally tested with lower spatial resolution.

3.1. Code Validation

Two-dimensional stability problem was solved with one wavelength ($Lx = 2\pi/\alpha$) domain size in the streamwise direction and the same velocity profile at every streamwise location to validate the numerical code written for the global instability analysis. Thus, $\dfrac{\partial U}{\partial x} = 0$ and $V = 0$. A ZPG ($\beta_H = 0$) boundary layer with the critical Reynolds number based on the displacement thickness $\mathrm{Re}_{\delta^*} = 580$ and the streamwise wave-number $\alpha_r = 0.179$ were taken to validate the approach [38]. To impose the wavelike behavior of the disturbances in the streamwise direction Robin's (Eq. (3.1)) and periodic (Eq. (3.2)) boundary conditions were applied. The same boundary conditions were applied in the wall normal direction for the local and global stability analyses [30]

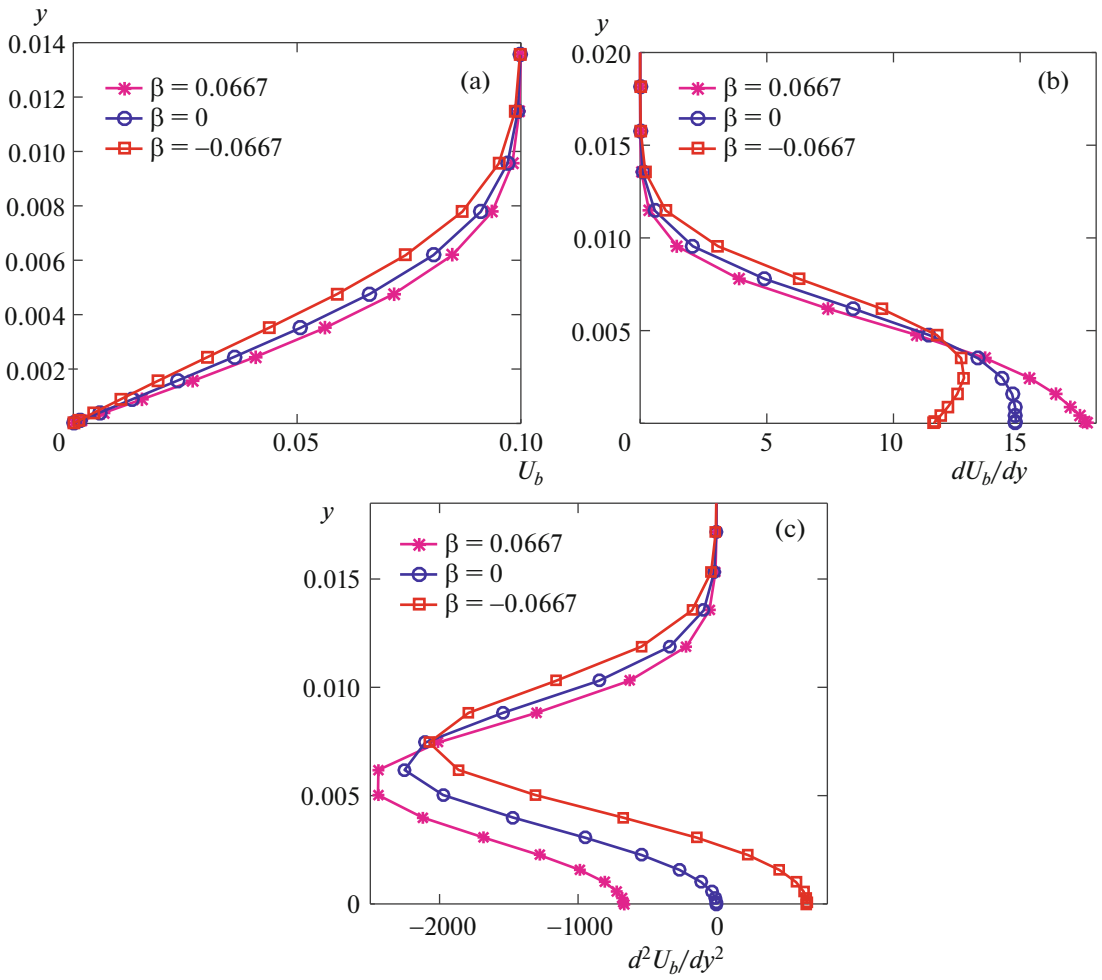

Fig. 2. Variation of U_b (a), $\frac{\partial U_b}{\partial y}$ (b), and $\frac{\partial^2 U_b}{\partial y^2}$ (c) for the FPG, APG, and ZPG at streamwise location $x = 0.5$ m. The positive value of β_H develops FPG and its negative values results in APG.

$$\frac{\partial^2 u_p}{\partial x^2} = -\alpha^2 u_p, \quad \frac{\partial^2 v_p}{\partial x^2} = -\alpha^2 v_p, \tag{3.1}$$

$$u_p(x, y) = u_p(x + Lx, y), \quad v_p(x, y) = v_p(x + Lx, y). \tag{3.2}$$

Figures 3a, 3b, and 3c present the comparison of the eigenspectrum and eigenfunctions for Re = 580 and $\alpha_r = 0.179$ for the global and local stability analyses. The eigenspectra and eigenfunctions computed using the global stability approach are found to be in excellent agreement with the local stability results of Mack [38]. Moreover, similar comparisons were done for the boundary layer instability for FPG with $\beta_H = 0.066$ and APG with $\beta_H = -0.066$. The comparison of the eigenspectra shown in Figs. 4a and 4b shows good agreement between the global and local stability analyses. The eigenfunctions of both approaches also are in good agreement (not shown here). Thus, the global stability results obtained using the Robin and periodic boundary conditions are in good agreement with the local stability approach.

3.2. Grid Convergence Study

To verify the independence and accuracy of the solutions for various grid sizes a test was performed. The numerical values of the two least stable eigenmodes computed for Re = 340 and the axisymmetric mode using completely different three grid sizes are shown in Table 1 The relative errors were computed

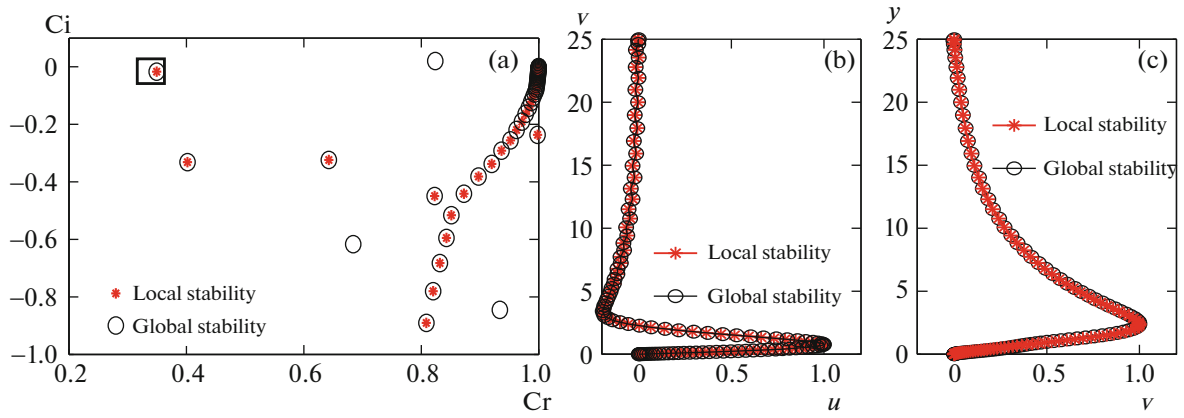

Fig. 3. Comparison of the eigenspectra (a), the streamwise eigenfunctions u (b), and the wall-normal eigenfunctions v (c) in the global and local stability analyses of 2D flat-plate boundary layers for Re = 580 and $\alpha_r = 0.179$ with ZPG. Here, Re = 580 is the critical Reynolds number for the local stability analysis.

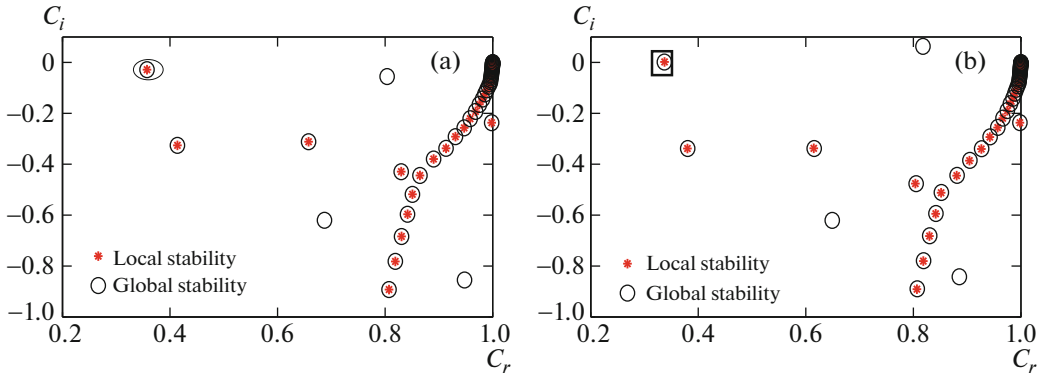

Fig. 4. Comparison of the eigenspectra for 2D flat-plate boundary layer at Re = 580 and $\alpha_r = 0.178$ obtained by the global and local stability approaches in the cases (a) of FPG ($\beta_H = 0.0667$) and (b) APG ($\beta = -0.0667$).

for the real and imaginary parts of the eigenvalues. The greatest computed error is considered. An increase in the spatial resolution shows monotonic convergence of the eigenvalues. The relative error for mesh # 1 is well within the limit and it is used for all the results reported here. The domain height $L_y = 25$ is sufficient in the wall normal direction to impose free-stream condition [27].

3.3. Effect of Streamwise Domain Length

The instability analysis of an open shear flow, like flat-plate boundary layer, in a finite domain length (truncated numerical domain) needs appropriate conditions at the exit of the domain. One should take

Table 1. The least stable eigenvalues ω_1 and ω_2 computed for various grid size at Re = 340 and $\beta_H = 0.044$. The streamwise and wall-normal domain sizes are $L_x = 420$ and $L_y = 20$. The successive grid refinement rate adopted was 1.1412

Mesh	$n \times m$	ω_1	ω_2	Error, %
1	251 × 61	$0.07049 - 0.01998i$	$0.07707 - 0.02009i$	3.450
2	193 × 53	$0.07045 - 0.01937i$	$0.07706 - 0.01942i$	6.353
3	171 × 47	$0.07043 - 0.01822i$	$0.07703 - 0.01826i$	–

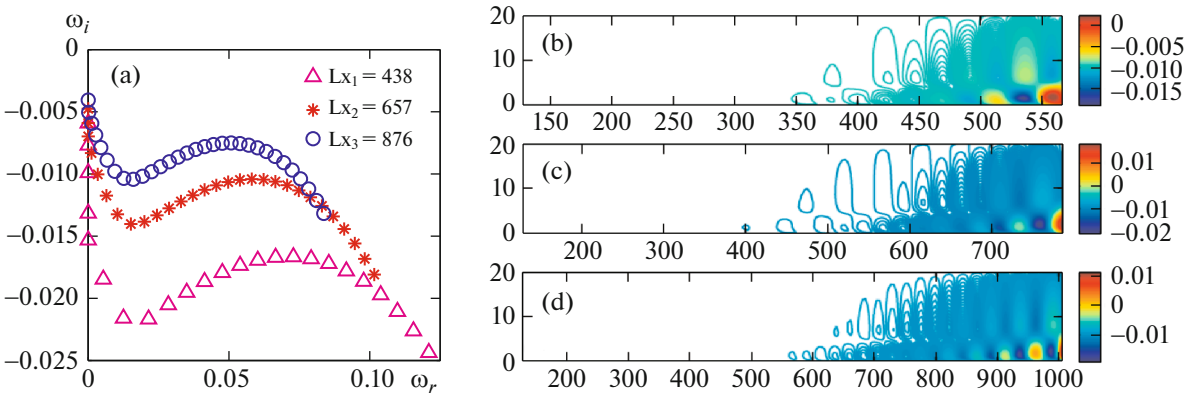

Fig. 5. Comparison of the eigenspectra for three different domain lengths for FPG with Re = 340 and $\beta_H = 0.0222$ (a) and comparison of the two-dimensional spatial structures of the real parts of u_p for $L_x = 438$ (b), 657 (c), and 876 (d).

care that the artificial boundary conditions should not affect the instability dynamics of such truncated domain. The global spectra of the truncated domain found in the open literature, such as boundary layers [28, 29], cylinder wakes [39, 40], and jets [41, 42], are highly dependent on the type and location of the exit conditions. To understand the effect of the streamwise domain length, we carried out a study for three different domain lengths.

Figure 5 shows the comparison of discrete parts of eigenspectra for three different domain lengths: 438, 657, and 876. The length is non-dimensionalized by the δ* at the inflow boundary of the domain. The comparison shows that the difference of the spectra depends on the streamwise domain length. The temporal growth rate increases with increase in the domain length for a given Reynolds number. In other words, the increased domain length increases the outflow Reynolds number which affects the temporal growth rate ω_i. The distribution of the frequency ω_r also depends on the streamwise domain length L_x. The distance between two consecutive frequencies ω_r reduces with increased domain length. Ideally, this distance reduces to zero, when the streamwise domain length is infinite. Thus, the eigenspectra presented here are functions of the numerical domain size. Figures 5a, 5b, and 5c show the two-dimensional spatial structure of the streamwise disturbance amplitudes, u_p for $\omega_r = 0.07028$ and Re = 340 with ZPG for L_x = 438, 657, and 876. The disturbances oscillate periodically and grow in size and magnitude in the flow direction while moving downstream.

3.4. Effect of Favorable PG

The spectra obtained from the solution of 2D eigenvalue problem for Re = 340 and FPG are shown in Fig. 6a. The discrete part of the eigenspectrum is shown here for different angles of incidence β_H. The least stable eigenmodes are marked by rectangles for different angles β_H. The global modes are found to be stable, since the imaginary parts of the least stable eigenmodes are negative. Figure 6a presents the comparison of the discrete parts of the eigenspectra corresponding to Tollmien—Schlichting (TS) waves with ZPG and FPG. It is found that an increase in the FPG increases the damping rate or reduces the temporal growth rate ω_i of the eigenmode having the greatest value of ω_i, which makes the global mode temporally more stable. This behavior is similar with the results of the parallel stability analysis. However, the distribution of the frequency for TS waves is not affected by the PG. It suggests that the FPG in the streamwise direction has an overall stabilizing effect. The least stable temporal eigenmodes ω_i were selected to study the spatial structure of the two-dimensional eigenmodes.

Figures 6d and 6e show the variation of the disturbance amplitudes in the flow direction at $y = 0.114$ and Re = 340 with different values of parameter β_H (FPG) for the least stable eigenmodes marked by rectangles in Fig. 6a. This eigenmode is oscillatory in nature because $\omega_r > 0$. The variation of the disturbance amplitudes, u_p and v_p, in the flow direction, as shown in Figs. 6d and 6e, are similar; however, the magnitude of the amplitudes reduces with the increased FPG (positive β_H). The wavelet structure of u_p and v_p disturbance amplitudes can be observable. The growth of disturbances takes place, while moving

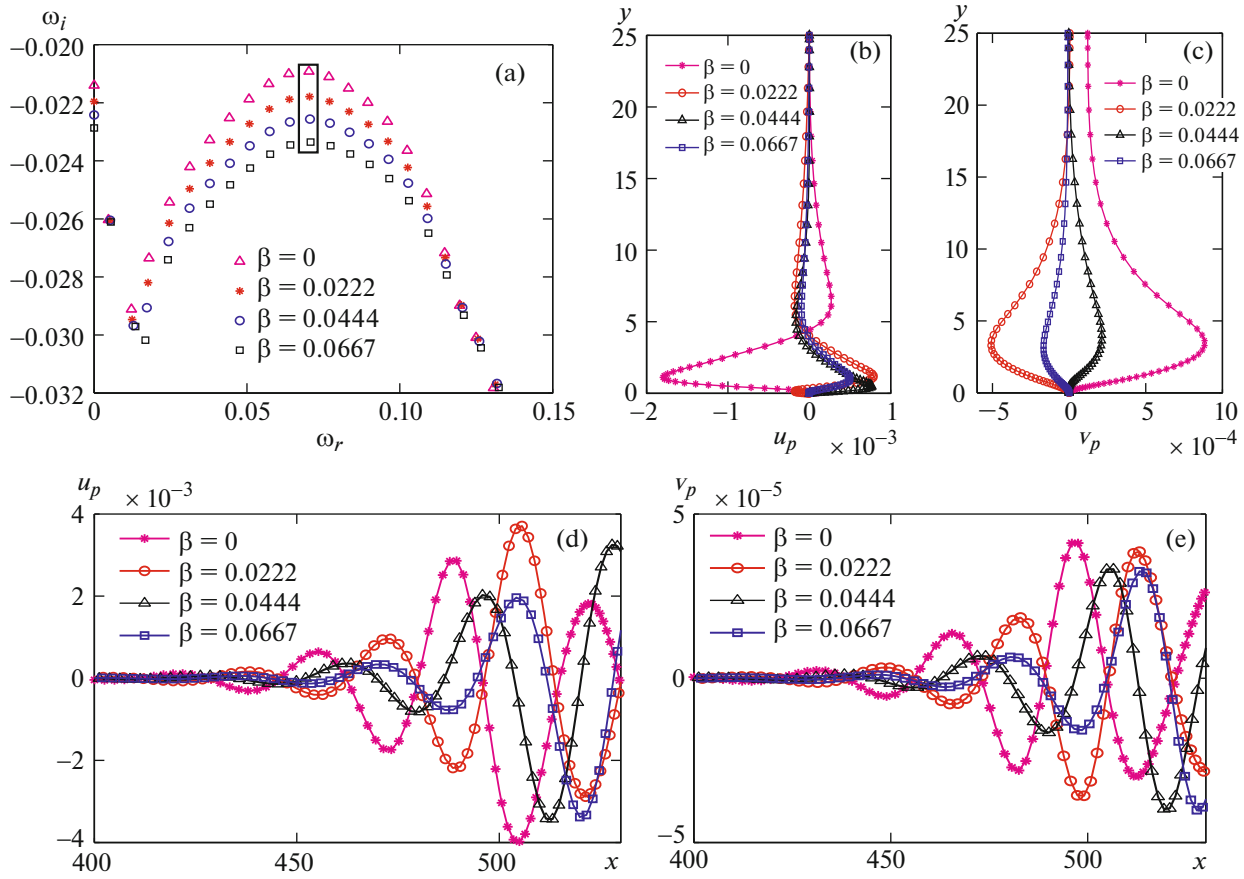

Fig. 6. Comparison of the eigenspectra (a), the variations of u_p (b) and v_p (c) in the y direction and the variations of u_p (d) and v_p (e) in the flow direction for different β_H at Re = 340 and $y = 0.114$ for FPG. Here, $\beta_H = 0$ is for ZPG and $\beta_H = 0.0222$, $\beta_H = 0.0444$, and $\beta_H = 0.0667$ are for FPG. The symbols: (△) $0.0702 - 0.0209i$, (∗) $0.0704 - 0.0217i$, (○) $0.0706 - 0.0225i$, (□) $0.0708 - 0233i$.

downstream with the base flow. It suggests that the flow is convectively unstable. The spatial structure of the disturbances was found to be similar with ZPG and FPG for boundary layer. The disturbances grow in size and magnitude when moving downstream. The disturbance magnitudes decrease with increase in β_H from 0.0222 to 0.0666. The development of the FPG reduces the disturbance amplitudes and, thus, the increased FPG has a stabilizing effect on the spatial growth of the disturbances.

Figures 6b and 6c show the variation of the u_p and v_p velocity disturbance amplitudes in the y direction at the streamwise location $x = 461$. The nature of the variation for the ZPG and FPG is found almost similar. At the wall, the disturbance amplitudes are zero due to the viscous effect, then it gradually increases in the y direction, and finally vanishes in the far field. It can be seen in Fig. 6 that the magnitudes of the u_p and v_p disturbances in the streamwise direction reduce with increase in PG. Thus, FPG also helps in spatially stabilizing the flow.

The growth or decay of the spatial eigenmodes takes place in the flow direction. To determine the growth/decay of all the disturbances in the flow direction, the spatial growth rate A_x was computed as follows:

$$A_x = \sqrt{\int_0^{y_{\max}} (u_p^*(x,y)u_p(x,y) + v_p^*(x,y)v_p(x,y))dy}, \tag{3.3}$$

where the asterisks denote the complex conjugate values.

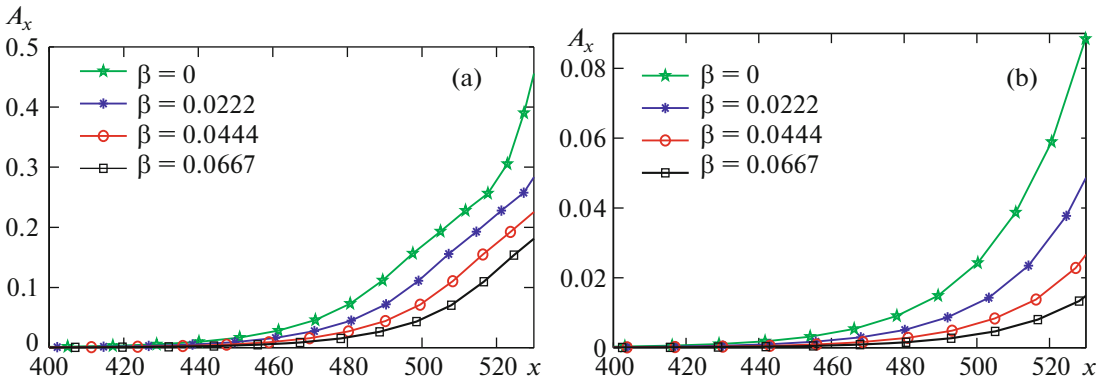

Fig. 7. Variations of the spatial amplification rate A_x for FPG in the flow direction for different values of β_H at Re = 340 (a) and Re = 480 (b). The value of A_x is calculated for the least stable global mode.

Figures 7a and 7b show the variation of the spatial amplification rate A_x for the velocity disturbances at different values of β_H and Reynolds numbers. The spatial growth rate A_x increases in the flow direction, as shown Fig. 7. It can be seen in Fig. 7 that, as the parameter β_H increases from 0.0222 (ZPG) to 0.0666 (FPG), A_x reduces in the flow direction. It proves that the development of the FPG in the streamwise direction reduces the spatial growth of the disturbances and hence it has overall stabilizing or damping effect on the spatial growth of the disturbances. It was also found that, as the Reynolds number increases from the 340 to 480, for the same PG the spatial growth rate reduces.

3.5. Effect of Adverse PG

We performed the global stability analysis for boundary layers with different adverse pressure gradient values. The eigenspectra of the boundary layer for different β_H values and Re = 340 with APG are shown in Fig. 8. The discrete parts of the eigenspectra are shown in Fig. 8a for different values of β_H. The least stable eigenmodes are marked by rectangles for each value of β_H and they are found to be negative. This implies that all global eigenmodes are temporally stable. This observation is in line with findings of [27], where the imaginary parts of the global modes are negative. Figure 8 presents the comparison of discrete parts of the eigenspectra corresponding to Tollmien—Schlichting (TS) waves for APG ($\beta_H > 0$). The temporal growth rate of the most unstable eigenmode increases with increase in β_H. It suggests that the APG in the flow direction has an overall destabilizing effect on the boundary layer. However, the distribution of the frequency is unchanged under the effect of PG. To study the spatial evolution of the two-dimensional disturbance amplitudes, the least stable eigenmodes were selected.

Figures 8b and 8c show the variation of the real parts of the u_p and v_p disturbance amplitudes for Re = 340 at $y = 0.114$ for different β_H values (APG). The least stable eiegenmodes with $\omega_r = 0.07$ were selected to study the spatial growth of the disturbance amplitudes. The least stable global modes are found to be globally stable, when $\omega_i < 0$, while the dimensionless frequency is almost the same for all the least stable global modes at different β_H values. It shows that the disturbance magnitudes increase, as they move downstream in the flow direction. The disturbance amplitudes have periodic nature in the flow direction. The magnitudes of the disturbance amplitudes increase, as the plate angle β_H varies from 0 to –0.06676. It proves that the development in the APG increases the spatial growth rate of the disturbance amplitudes. Thus, the APG has a destabilizing effect on the boundary layer.

Figure 9 shows the variation of spatial amplification rate A_x of the velocity disturbance amplitudes for different plate angles β_H and Reynolds numbers. The spatial amplification rate A_x increases in the flow direction and with increase in APG. The APG has an overall destabilizing effect on the disturbance amplitudes and, therefore, on the boundary layer as a whole.

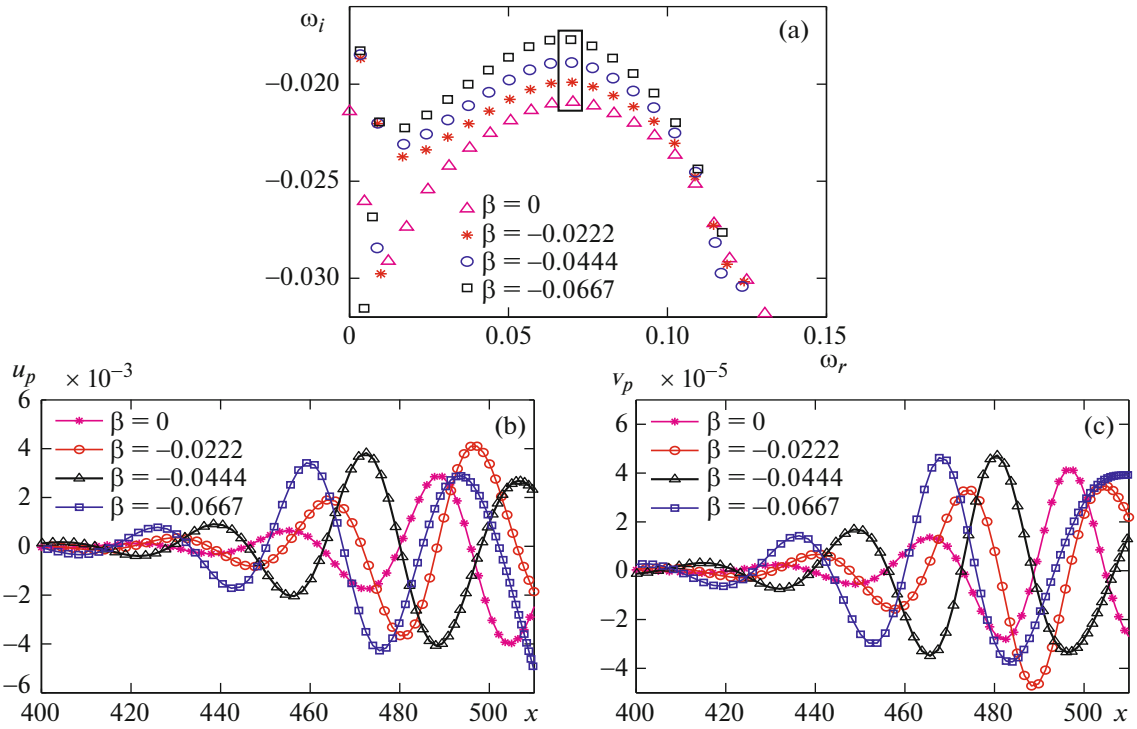

Fig. 8. Comparison of the eigenspectra (a), the streamwise disturbance amplitudes u_p (b), and the wall-normal disturbance amplitudes v_p (c) for different β_H at Re = 340 and $y = 0.114$. Here, $\beta_H = 0$ is for ZPG and $\beta_H = -0.022$, $\beta_H = -0.044$, and $\beta_H = -0.0667$ are for APG. Symbols: (△) $0.0696 - 0.0177i$, (∗) $0.0698 - 0.0188i$, (○) $0.0700 - 0.0199i$, (□) $0.0702 - 0209i$.

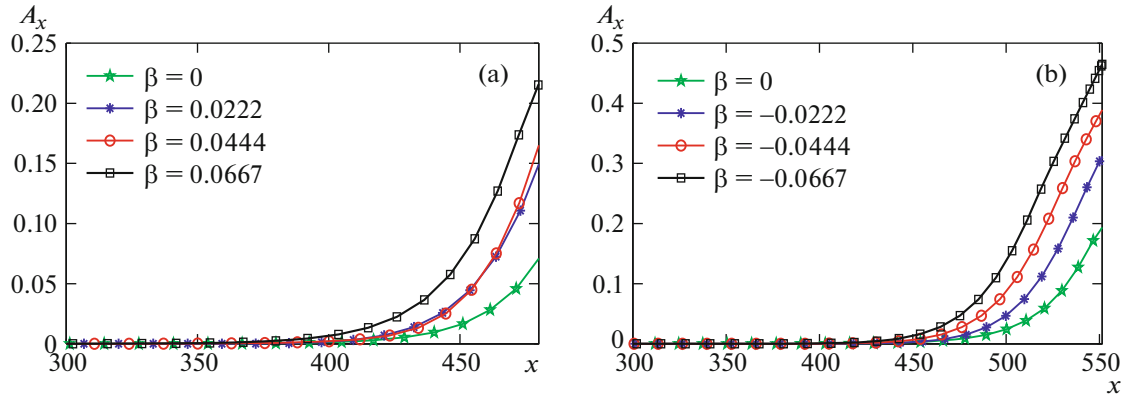

Fig. 9. Variation of the spatial amplification rate A_x for APG in the flow direction for different values of β_H at Re = 340 (a) and Re = 480 (b). The value of A_x is calculated for the least stable global mode.

SUMMARY

The global stability analysis is performed for an incompressible boundary layer developed on an inclined flat plate in the presence of streamwise PG. The various incident angles β_H considered are 0.0222, 0.0444, and 0.0667. The two-dimensional eigenvalue problem is solved numerically using Arnoldi's iterative algorithm. The computed global modes are stable because the largest imaginary parts of the eigenvalues ω_i are found to be negative. The spatial structure of the disturbance amplitudes shows that they grow in size and magnitude as they move downstream. The frequency distribution remains

almost the same for negative and positive pressure gradients. As the positive angle β_H increases from 0 to 0.0667, the temporal growth rate ω_i and the spatial growth rate reduce, which makes the global modes more stable. Thus, FPG makes the flow temporally and spatially more stable. As the negative value of β_H increases from 0 to −0.0667, the temporal growth rate ω_i increases and the global modes become less stable. The spatial growth rate A_x also increases in the streamwise direction. Thus, the development of the APG makes the global modes less stable. Overall, FPG has a damping and APG has an amplifying effect on the disturbances. Thus, the disturbances amplify when subjected to APG and decay when subjected to FPG. The effect of domain length is also studied in the analysis; it is found that the global stability strongly depends on the streamwise domain size.

DECLARATION OF CONFLICTING INTERESTS

The Author declares no potential conflicts of interest with respect to the research, authorship, and/or publication of this article.

REFERENCES

1. H. J. Obremski, M. V. Morkovin, and M. Landahl, "A portfolio of stability characteristics of incompressible boundary layer," AGARDograph 134 (1969).
2. E. R. Van Driest and C. B. Blumer, "Boundary layer transition: freestream turbulence and pressure gradient effect," AIAA J. **1**, 1303–1306 (1963).
3. S. K. Saxena and T. K. Bose, "Numerical study of effect of pressure gradient on stability of an incompressible boundary layer," Phys. Fluids **17**, 1910–1912 (1974).
4. T. C. Corke and S. Gruber, "Resonant growth of three-dimensional modes in Falkner-Skan boundary layers with adverse pressure gradient," J. Fluid Mech. **320**, 211–233 (1996).
5. C. Liu and S. A. Maslowe, "A numerical investigation of resonant interactions in adverse pressure gradient boundary layers," J. Fluid Mech. **378**, 269–289 (1999).
6. B. J. Abu-Ghannam and R. Shaw, "Natural transition of boundary layers- the effects of turbulence, pressure gradient, and flow history," J. Mech. Engng. Sci. **22**, 213–228 (1980).
7. J. P. Gostelow, A. R. Blunden, and G. J. Walker, "Effect of free-stream turbulence and adverse pressure gradients on boundary layer transition," J. Turbomach. **116**, 392–404 (1994).
8. N. Vinod and R. Govindarajan, "Pattern of breakdown of laminar flow into turbulent spots," Phys. Rev. Lett. **93**, 114501 (2004).
9. N. Vinod and R. Govindarajan, "The signature of laminar instabilities in the zone of transition to turbulence," J. Turbulence **8**(2), (2007).
10. R. Narasimha, "The laminar-turbulent transition zone in the boundary layer," Progr. Aero. Sci. **22**, 29–80 (1985).
11. A. Seifert and H.P. Hodson, "Periodic turbulent strips and calmed regions in a transitional boundary layer," AIAA J. **37**, 1127–1129 (1999).
12. S. A. Maslowe and R. J. Spiteri, "The continuous spectrum for a boundary layer in a streamwise pressure gradient," Phys. Fluids **13**, 1294 (2001).
13. Y. H. Zurigat, A. H. Nayfeh, and J. A. Masad, "Effect of pressure gradient on the stability of compressible boundary layers," AIAA J. **30**, 2204–2211 (1992).
14. K. J. Franko and S. Lele, "Effect of adverse pressure gradient on high speed boundary layer transition," Phys. Fluids **26**, 24106 (2014).
15. W. Zhang, H. Yang, D. Hua-Shu, and Z. Zuchao, "Flow unsteadiness and stability characterstics of low-Re flow past an inclined triangular cylinder," J. Fluids Eng. **139**, 121203 (2017).
16. R. L. Kimmel, "The effect of pressure gradients on transition zone length in hypersonic boundary layer," Flight Dynamics Directorate (1993).
17. N. Itoh, "Effect of pressure gradients on the stability of three-dimensional boundary layers," Fluid Dynamic Research **7**, 37–50 (1991).
18. M. W. Johnson and A. Pinarbasi, "The effect of pressure gradients on boundary layer receptivity," Flow, Turbulence and Combustion **93**, 1–24 (2014).
19. J. A. Masad and Y. H. Zurigat, "The effect of pressure gradients on first mode of instability in compressible boundary layer," Phys. Fluids **6**, 3945 (1994).
20. A. Tumin and D. E. Ashpis, "Optimal dsturbances in boundary layers subject to streamwise pressure gradient," 33rd AIAA Fluid Dynamics Conf. (2003).

21. J. P. Gostelow and A. R. Blunden, "Investigation of boundary layer transition in an adverse pressure gradient," ASME J. Turbomachinery **111**, 366–374 (1989).
22. S. Igarashi, H. Sasaki, and M. Honda, "Influence of pressure gradient upon boundary layer stability and transition," Acta Mechanica **73**, 187–198 (1988).
23. R. Govindarajan and R. Narasimha, "Stability of spatially developing boundary layers in pressure gradients," J. Fluid Mech. **300**, 117–147 (1995).
24. G.J. Walker and J. P. Gostelow, "Effect of adverse pressure gradients on the nature and length of boundary layer transtion," Gas Turbines and Aeroengine Congress and Exposition (1989).
25. L. Chonghui, "A numercal investigation of instability and transition in adverse pressure gradient boundary layers," Ph.D. Thesis, McGill University, Montreal (1997).
26. P Corbett and A. Bottaro, "Optimal perturbations for boundary layers subject to streamwise pressure gradient," Phys. Fluids **12**, 120–131 (2000).
27. F. Alizard and J. C. Robinet, "Spatially convective global modes in a boundary layer," Phys. Fluids **19**, 114105 (2007).
28. U. Ehrenstein and F. Gallaire, "On two-dimensional temporal modes in spatially evolving open flow: the flat-plate boundary layer," J. Fluid Mech. **536**, 209–218 (2005).
29. E. Akervik, U. Ehrenstein, F. Gallaire, and D. S. Henningson, "Global two-dimensional stability measure of the flat plate boundary-layer flow," Eur. J. Mech. B/Fluids **27**, 501–513 (2008).
30. R. Bhoraniya and N. Vinod, "Global stability analysis of axisymmetric boundary layer over a circualr cylinder," Theor. Comput. Fluid Dyn. **32**, 425–449 (2018).
31. R. Bhoraniya and N. Vinod, "Global stability analysis of axisymmetric boundary layer over a circular cone," J. Phys.: Conf. Ser. **822**, 012018 (2017).
32. R. Bhoraniya and N. Vinod, "Global stability analysis of axisymmetric boundary layer over a circular cone," Phys. Rev. Fluids **02**, 063901 (2017).
33. V. Theofilis, "Advances in global linear instability analysis of nonparallel and three-dimensional flows," Progr. Aerospace Sci. **39**, 249–315 (2003).
34. H. Fasel, U. Rist, and U. Konzelmann, "Numerical investigation of the three-dimensional development in boundary layer transition," AIAA J **28**, 29–37 (1990).
35. G. Swaminathan, Kirti. Shahu, A. Sameen, and R. Govindarajan, "Global instabilities in diverging channel flows," Theor. Comput. Fluid Dyn. **25**, 53–64 (2011).
36. M. R. Malik, "Numerical methods for hypersonic boundary layer stability," J. Comput. Phys. **86**(2), 376–412 (1990).
37. B. Costa, W. S. Don, and A. Simas, "Spatial resolution properties of mapped spectral Chebyshev methods," Proceedings of SCPDE, 179–188 (2007).
38. L. M. Mach, "A numerical study of temporal eigenvalue spectrum of the Blasius boundary layer." J. Fluid Mech. **73**, 497–520 (1976).
39. D. Sipp and D. Lebedev, "Global stability of base and mean flows: a general approach to its applications to cylinder and open cavity flow," J. Fluid Mech. **593**, 333–358 (2007).
40. O. Marquet, D. Sipp, and D. Lebedev, "Sensitivity analysis and passive control of cylinder flow," J. Fluid Mech. **615**, 221–252 (2008).
41. J. W. Nichols and S. K. Lele, "Global modes and transient response of a cold supersonic jet," J. Fluid Mech. **669**, 225–241 (2011).
42. X. Garnaud, L. Lesshafft, P. J. Schimd, and P. Huerre, "Modal and transient dynamics of jet flows," Phys. Fluids. **25**, 044103 (2013).